ROYAL SOCIETY OF CHEMISTRY

PAPER

Check for updates

Stimuli-responsive helical polymeric particles with amplified circularly polarized luminescence†

Huimin Duan,[ab] Hongkun Pan,[ab] Jiawei Li [ID] *[abc] and Dongming Qi [ID] *[abc]

The stimuli-responsive circularly polarized luminescence (CPL) property is highly desirable for the development of advanced multifunctional optical materials. However, the fabrication of CPL solid materials showing stimuli-responsive behavior in terms of tuning and amplifying the luminescence dissymmetry factor (g_{lum}) remains a great challenge owing to the disorder and aggregation-caused quenching of solid aggregates. Herein, novel solid-state stimuli-responsive CPL helical polymeric particles (SRCHPs) with a fully conjugated skeleton have been successfully fabricated *via* the precipitation copolymerization of chiral and fluorescent propargylamide monomers. The SRCHPs exhibit stimuli-responsive intense circular dichroism, fluorescence emission, and amplified CPL effects under temperature, pH, and polarized light stimulation conditions. This is attributed to the coordination of the intramolecular hydrogen bonding and conjugated $\pi-\pi$ stacking interactions at a large scale based on the cis-transoidal dynamic helical structure, resulting in the amplification of chirality and circularly polarized energy. The present study reports a promising CPL stimuli-responsive and amplification process in the solid state based on a special main-chain conformation to achieve a simultaneous improvement in chirality and fluorescence.

Introduction

Due to their remarkable potential applications in changeable photoemission sensors, 3D optical displays, CPL dynamic switching, optical amplifiers, data storage, multiple encryption and anti-counterfeiting, stimuli-responsive circularly polarized luminescent (CPL) materials are attracting widespread attention.[1–5] Currently, a number of stimuli-responsive CPL materials with a high luminescence dissymmetry factor (g_{lum}) have been favored and fabricated *via* approaches utilizing the dynamic assembly of liquids,[6] light emitting molecule-binding chiral centers,[7] metal-induced complexes,[8] energy level-assisted photonic inversion,[9] anion-triggered switching,[10] *etc.* Nevertheless, the fabrication of stimuli-responsive CPL materials with changeable $|g_{lum}|$ and flexible design in the solid state remains a great challenge because of the disorder and aggregation-caused quenching (ACQ) of solid aggregates.[11,12]

One of the most promising highly polarized stimuli-responsive CPL materials in the solid state are supramolecular polymers that can adapt to their environment, with the properties of dynamic and chiral amplification.[13–16] As a result, chiral fluorescence supramolecular polymeric particles, which combine the two key factors namely "chirality" and "fluorescence" on the same dynamic polymer chain and further integrate the three significant factors namely "chirality," "fluorescence," and "particulate morphology" into one solid-state whole,[17,18] exhibit significant applications in stimuli-responsive CPL solid-state systems.

Among various chiral polymer structures, conjugated polymers expectantly provide many construction strategies[19,20] for CPL supramolecular materials with high polarization and sensitive responsiveness due to their high molar extinction coefficient in the UV-vis regions[21] and fine-tunable emission wavelengths.[22] Therefore, the key to preparing stimuli-responsive CPL solid materials with high $|g_{lum}|$ values and high luminous quantum efficiency is designing conjugated structures to enhance chiral amplification, improve the conjugated degree of the total frame between the main chain and the side group to eliminate the ACQ effect and tune CPL properties to achieve changeable $|g_{lum}|$.[23,24] As a typical dynamic conjugated polymer, helical substituted polyacetylene possesses easily tunable helical main chains under external stimuli, flexible designability, and photoelectric properties,[25–27] resulting in excellent and stimuli-responsive CPL activity. The preferably one-handed helical conformation

a Key Laboratory of Advanced Textile Materials and Manufacturing Technology, Ministry of Education, Zhejiang Sci-Tech University, Hangzhou, 310018, P. R. China. E-mail: jiaweili@zstu.edu.cn, dongmingqi@zstu.edu.cn; Fax: +86 571-86843255; Tel: +86 571-86942702

b Zhejiang Provincial Engineering Research Center for Green and Low-carbon Dyeing & Finishing, Zhejiang Sci-Tech University, Hangzhou, 310018, P. R. China

c Zhejiang Provincial Innovation Center of Advanced Textile Technology, Shaoxing, 312000, China

† Electronic supplementary information (ESI) available. See DOI: https://doi.org/10.1039/d2tc04292d
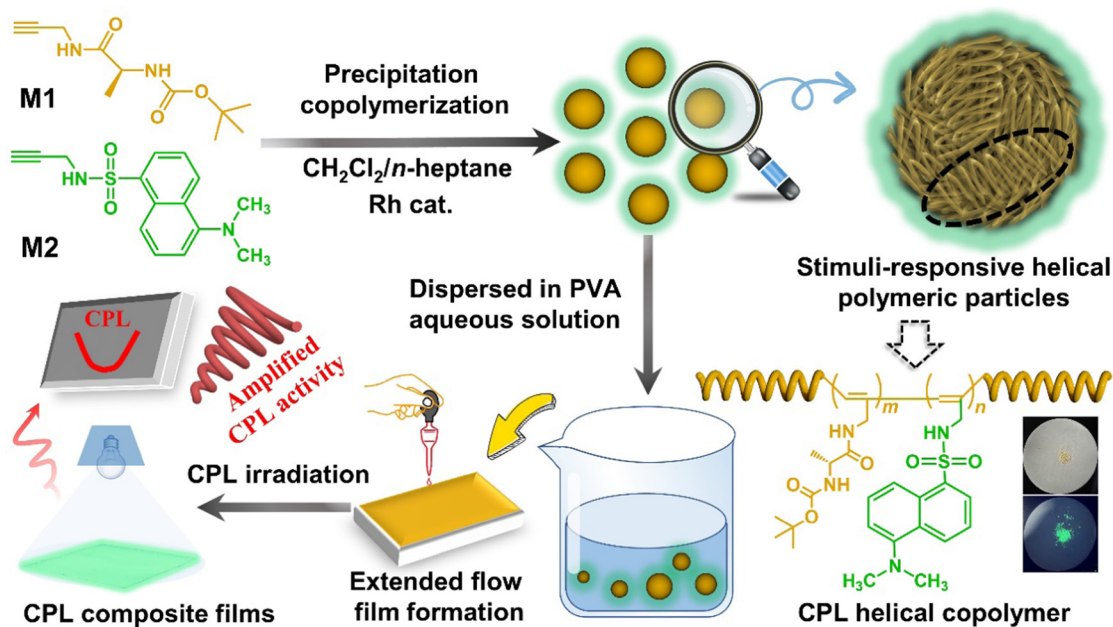
Scheme 1 Schematic illustration for constructing stimuli-responsive helical polymeric particles and composite films with amplified CPL.

of the polymer backbone is the key to generating the CPL property, exhibiting "chiral amplification" and "energy absorption" effects in the main chain.[28–30] These features endow them with great potential to tune and enhance the CPL properties in the construction of stimuli-responsive CPL solid materials. However, as far as we know, such supramolecular polymeric solid particles with stimuli-responsive CPL properties based on dynamic helical structures have been rarely reported.

In this work, we constructed stimuli-responsive CPL helical polymeric particles (SRCHPs) with conjugate frames based on the cis-transoidal conformation *via* the precipitation copolymerization of amino acid amide chiral and dan sulfonamide fluorescent acetylene monomers (Scheme 1). The precipitation copolymerization method was chosen because it does not involve emulsifiers or stabilizers.[31,32] Amide monomers were used to provide intramolecular hydrogen bonds and chirality. Aromatic groups provided conjugated structures and fluorescence properties. A conjugated link was formed between the side aromatic group and the alternating single–double bond conjugate structure. Subsequently, under the action of an intramolecular hydrogen bond, the main chain was twisted into a special *cis* helical structure, which provides a positive "bridge" for the simultaneous transmission and amplification of chiral and fluorescence properties. We selected the copolymerization of chiral and fluorescent monomers to construct novel controllable chiral fluorescent materials to expediently adjust the chiral and fluorescent components. The SRCHPs exhibited stimuli-responsive CPL properties with respect to temperature and pH as well as certain optical encryption and anti-counterfeiting functions. Accordingly, this study not only provides a simple and regulatable strategy for stimuli-responsive CPL solid materials but also expands to a type of supramolecular polymer material with amplified CPL properties.

Experimental

Materials

Organic solvents, including dichloromethane (DCM), ethanol, tetrahydrofuran (THF), ethyl acetate (EA), *n*-heptane and *n*-hexane were dried over molecular sieves and distilled under reduced pressure before use. Dansyl chloride, Boc-L-alanine, and propargylamine were purchased from Aldrich (Sigma-Aldrich, USA) and used without further purification. The chiral substituted acetylene monomer (M-L-ala-Boc, M1) and the fluorescent achiral substituted acetylene monomer (M-DA, M2) were synthesized according to previous reports.[31,33] The catalyst (nbd)Rh$^+$B$^-$(C$_6$H$_5$)$_4$ was prepared with a high yield (78%) following a literature procedure.[34] Poly(vinyl alcohol) (PVA, average M_w = 2 50 000) was purchased from JVP.

Measurements

FT-IR spectra were recorded using a Nicolet 5700 infrared spectrometer (Thermal Power Company, American, KBr pellet method). An Avance AV 400 MHz spectrometer (Bruker, Switzerland) was used to record the ^{1}H NMR and ^{13}C NMR spectra. The number-average molecular weight (M_n) and molecular weight polydispersity (PDI, M_w/M_n) were determined *via* GPC (Waters 515 Shim-pack GPC-804 column, USA) with dimethylformamide (THF) as the eluent and polystyrene as the calibration standard. A DSM 172 spectrophotometer (OLIS, USA) equipped with a Peltier light source and a water-circulating temperature controller was used to perform circular dichroism (CD), UV-vis absorption, and CPL spectroscopy. Specific rotations were measured using a P-2000 digital polarimeter (JASCO, Japan, sodium D-line, 589 nm) at room temperature. An F-4600 fluorescence spectrophotometer (HITACHI, Japan) with an excitation wavelength of 365 nm and a bandwidth of 10 nm was used to record the fluorescence spectra.

This journal is © The Royal Society of Chemistry 2023

J. Mater. Chem. C, 2023, **11**, 172–182 | **173**

The fluorescence quantum yield was obtained on an FLS1000 steady-state transient fluorescence spectrometer (Edinburgh, UK). A LabRAM HR Evolution instrument (Horiba Scientific, Japan) at λ = 325 nm under laser pulses was used to record the Raman spectra. Differential scanning calorimetry (DSC) traces were measured under a N_2 atmosphere at a heating rate of 10 °C min^{-1} using a TA DSC Q2000 differential scanning calorimeter.

Preparation of helical polymeric particles (P_X)

A typical precipitation copolymerization strategy was used to prepare helical polymeric particles. A nonfluorescent chiral monomer (M1) underwent copolymerization with an achiral fluorescent monomer (M2) in the presence of (nbd)Rh$^+$B$^-$(C$_6$H$_5$)$_4$ with an M1/M2 mass ratio of m/n, X = 5:5, 6:4, 7:3, 8:2, and 9:1, which were termed P_{55}, P_{64}, P_{73}, P_{82}, and P_{91}, respectively. Taking P_{55} as an example, with an M1/M2 mass ratio of 5:5, a large mixture of monomers (M1 and M2, [M] = 0.025 M; as a representative) and (nbd)Rh$^+$B$^-$(C$_6$H$_5$)$_4$ ([Rh] = 2.5 × 10^{-4} M) was separately added to two tubes. CH$_2$Cl$_2$ (0.5 mL) was added to the monomer tube and the catalyst tube. After complete dissolution of the monomers and catalyst, the catalyst solution was immediately transferred to the tube containing the monomers. Then, n-heptane was slowly added to the reaction tube. The polymerization was performed under N_2 at 30 °C for 3 h. After filtration, the product was washed with n-hexane three times and dried in a vacuum to obtain P_{55} particles. Other particles were copolymerized in a similar manner.

Preparation of chiral fluorescent composite films

By uniformly dispersing copolymer P_X into the PVA solution, composite films of the helical polymeric particles were prepared. Taking the chiral fluorescent composite films of P_{55} as an example, P_{55} (0.05 g) was dispersed in 5 mL of PVA (0.5 g) aqueous solution and cast in a polytetrafluoroethylene mold to form a film. The H$_2$O was then evaporated at room temperature to obtain a uniform film with a thickness of ∼0.5 mm. Similar composite films were prepared with P_{64}, P_{73}, P_{82} and P_{91} via the above method.

Results and discussion

Synthesis of helical polymeric particles

Herein, we synthesized novel chiral fluorescent polymeric particles (P_X) with one-handed helical polymer chains via the precipitation copolymerization of a chiral monomer with an achiral fluorescent monomer (Scheme 1).

The chemical and structural characterization studies of M1, M2, and the copolymeric particles P_X are displayed in Fig. 1a–c. The characteristic peaks for the –C≡C bonds of M1 (2124 cm^{-1}) and M2 (2121 cm^{-1}) both disappeared in the FT-IR spectrum of the copolymeric particles (Fig. 1a). Similarly, the particular chemical shifts for the –HC≡ moiety of M1 (δ_H 2.35 ppm, δ_C 68.7 ppm) and M2 (δ_H 1.95 ppm, δ_C 46.5 ppm) were not observed in the ^{1}H NMR (Fig. 1b) and ^{13}C NMR (Fig. 1c) spectra of the copolymeric particles. Ultimately, through

precipitation copolymerization, the copolymeric particles with the target structure were obtained smoothly.

As the precipitation copolymerization of two acetylene-derived monomers was investigated to prepare chiral fluorescence particles, the driving forces and influencing factors during the formation process of the novel particles were derived from five aspects: the mixed solvent ratio (Fig. 1d–g, Fig. S1, and Table S1, ESI†), the growth time (Fig. S2 and Table S2, ESI†), the total monomer concentration (Fig. S3a–c, S4, and Table S3, ESI†), the Rh catalyst concentration (Fig. S3d–f, S5, and Table S4, ESI†) and the feed mass ratio of the two monomers M1/M2 (Fig. S3g–l, S6, S7, and Table S5, ESI†). First, when the CH$_2$Cl$_2$/n-heptane ratios were 1/6, 1/8, and 1/9 (mL/mL) (Fig. 1d, f, and g), the P_{55} particles exhibited a non-uniform and regular morphology. The optimum solvent system CH$_2$Cl$_2$/n-heptane ratio was 1/7 (mL/mL) (Fig. 1e). Its SEM images present a regular morphology (∼630 nm in diameter). This was due to an excess of good solvent or poor solvent, both of which resulted in particles with pronounced agglomeration. Second, according to the SEM images, yield, and average diameter of the particles (Fig. S2 and Table S2, ESI†), the mechanism of particle growth is summarized into three stages: copolymer chain formation (5–10 min), nucleation of the copolymer (10–30 min) and particle formation (45–120 min).[31,32] Third, based on the results from Fig. S3a–c, S4, and Table S3 in the ESI,† the best total monomer concentration was 2.5 × 10^{-2} M. The concentration was too low to form longer copolymer chains, and a higher concentration made the copolymer chain precipitate rapidly from the poor solvent, which affected the nucleation stage. Fourth, the appropriate Rh catalyst concentration was 2.5 × 10^{-4} M ([M]/[Rh] = 100/1), and the M_n of the copolymer was found to be 4.9 × 10^3 g mol^{-1} with a PDI of 1.6 via GPC data analysis (Fig. S5 and Table S4, ESI†). Finally, the mass ratio M1/M2 had a visible effect on the spheroidization of the copolymer, as shown in the SEM images in Fig. S3g–l (ESI†); however, there was still a tendency to form a microsphere morphology. Under these optimal conditions (mixed solvent CH$_2$Cl$_2$/n-heptane ratio of 1/7 (mL/mL), growth time of 45 min, total monomer concentration of 2.5 × 10^{-2} M, Rh catalyst concentration of 2.5 × 10^{-4} M, and feed mass ratio of the two monomers M1/M2 of 5:5), helical polymeric particles with a regular size (average diameter, 630 nm) and good optical properties (see below) were prepared in high yields of 85.4–89.2%.

Optical activity, fluorescence, and CPL properties

In line with previous reports,[35,36] the resulting helical polymeric particles from precipitation polymerization were obtained as a visible yellowish white solid powder (Scheme 1). This tentatively indicates that the P_X chains forming the particles took on a helical conformation, since substituted polyacetylenes, even micro–nanoparticles with helical structures, demonstrate a yellowish white color. The $[\alpha]_D$ information presented in Table S5 (ESI†) also supports the above conclusion. Therefore, to further prove this conclusion, we characterized the conformation of the particles via CD and UV-vis absorption spectroscopy as these are typical methods to characterize the secondary structure of helical
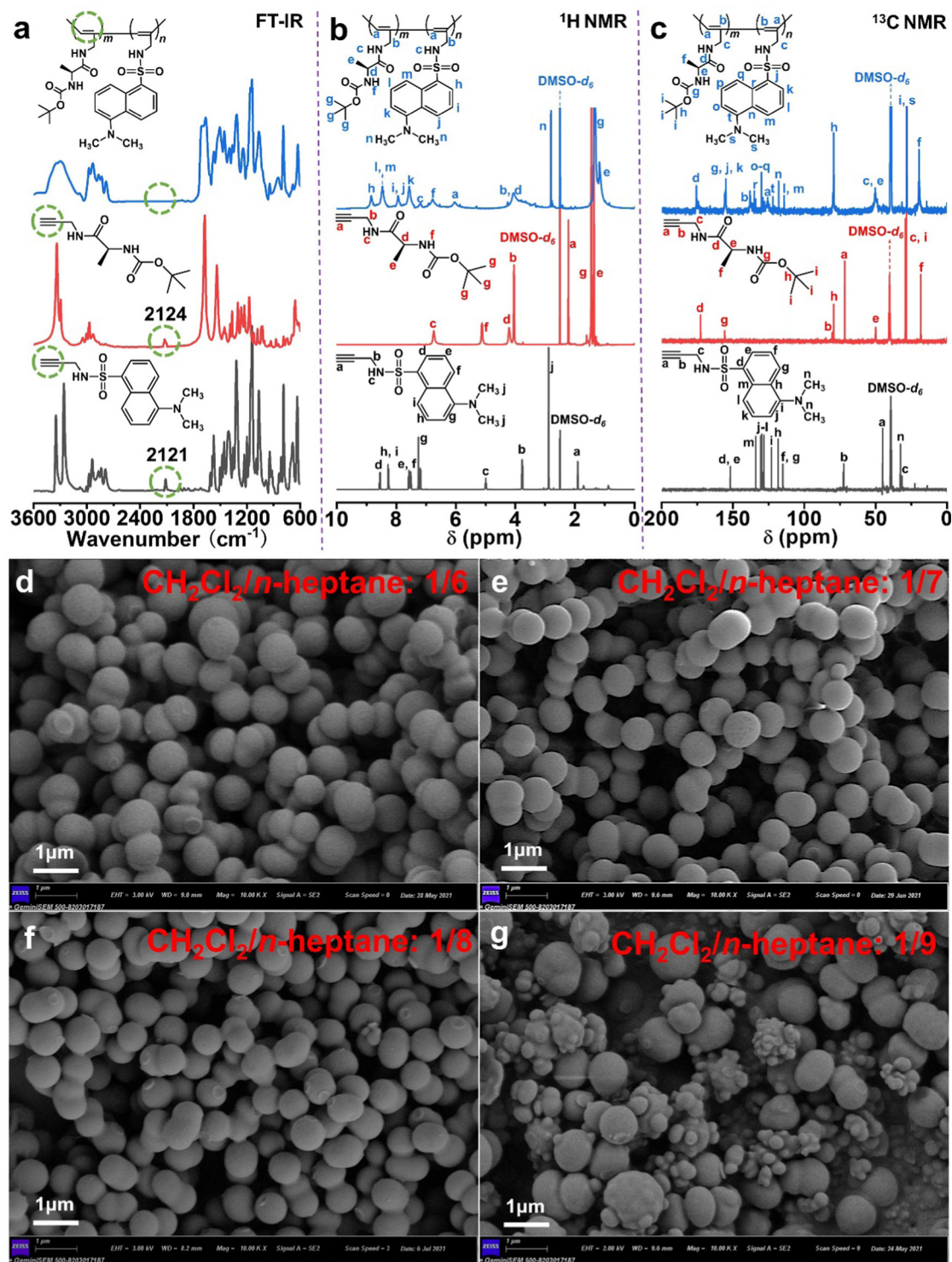
174 | *J. Mater. Chem. C*, 2023, **11**, 172–182

This journal is © The Royal Society of Chemistry 2023

Fig. 1 (a) Typical FT-IR spectra (KBr pallet), (b) ^{1}H NMR and (c) ^{13}C NMR spectra in DMSO-d_6 of M2, M1 and P_{55} particles, SEM images of P_{55} particles prepared in CH_2Cl_2/n-heptane with varying ratios: (d) 1/6; (e) 1/7; (f) 1/8; (g) 1/9 (mL/mL). Other conditions as shown in Table S1 (ESI†).

polymers.[37,38] In order to maintain the spherical morphology of particles in the test, we recorded the CD and UV-vis absorption spectra (Fig. 2a) of the P_X particles by dispersing them in a certain PVA aqueous solution to prepare composite films, as the P_X particles were insoluble in water. When substituted

polyacetylenes adopt a predominant handed helical conformation,[36,39,40] they usually show obvious CD signals and UV-vis absorption peaks. P1 possessed a notable CD signal at around 400 nm, and P_X had an intense CD signal at different wavelengths. In the UV-vis absorption spectra, the absorption peak

This journal is © The Royal Society of Chemistry 2023

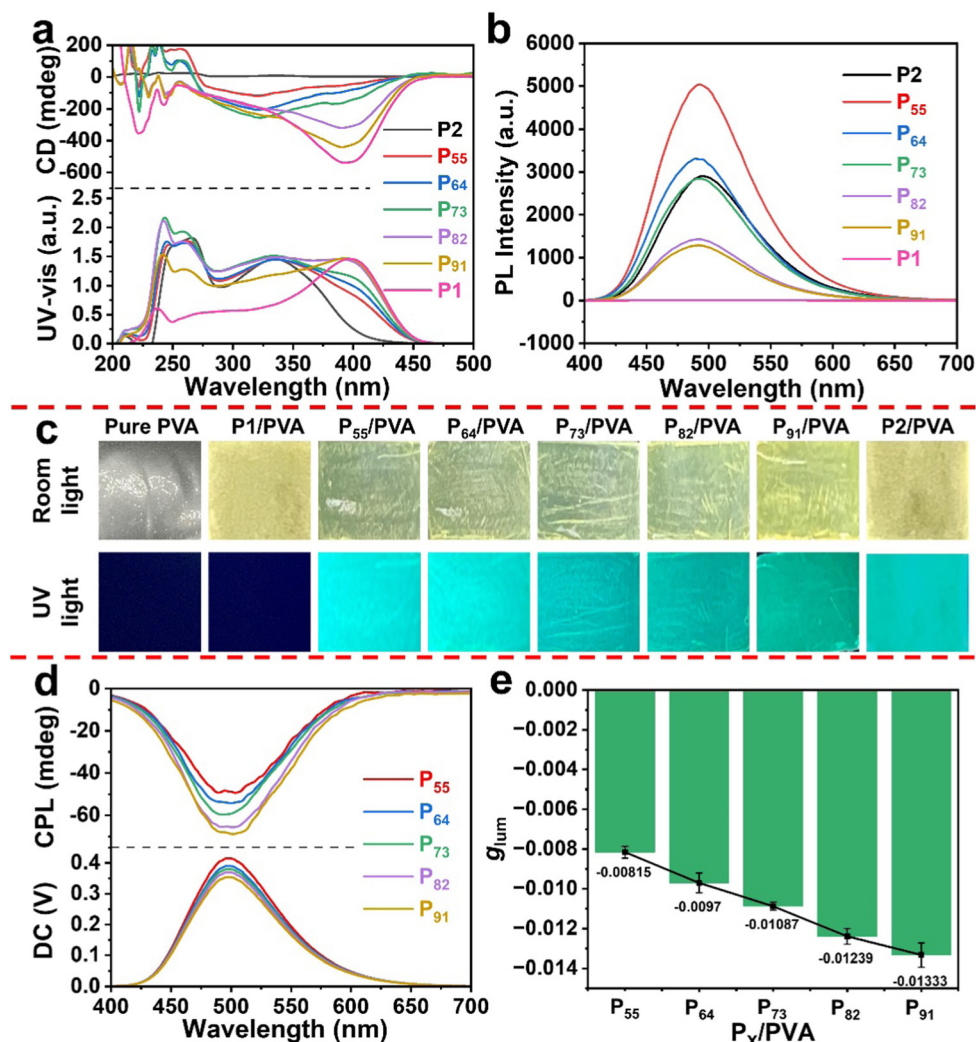J. Mater. Chem. C, 2023, 11, 172–182 | 175

Fig. 2 (a) CD and UV-vis absorption spectra, (b) fluorescence emission excited at 365 nm, and (c) photo images of P1/PVA, P2/PVA and P_X/PVA composite films; (d) circularly polarized fluorescence spectra (CPL) and (e) CPL dissymmetry factor g_{lum} versus wavelength both excited at 365 nm for P_X/PVA composite films.

was at the wavelength corresponding to the CD spectra. However, due to the absence of the chirality in M2, P2 exhibited a null CD effect in the polymer backbone region (Fig. S8, ESI†), indicating that it adopted a racemic helical structure. Interestingly, compared with P1, the CD effect of P_{91}/PVA exhibited a broader UV region belonging to the polymer backbone region. P_{82}/PVA and P_{73}/PVA also presented similar phenomena. With a decrease in chiral components, the UV absorption of the copolymeric particles blue-shifted from 400 to 340 nm; meanwhile, their CD signals also blue-shifted to the corresponding wavelengths and became weakened. The above results not only illustrate that particles with different one-handed helical conformations were obtained but also explain that the critical factor affecting the construction of copolymeric particles with different degrees of preferential helicity is the chiral content. These $[\alpha]_D$ results also offer notable support to the above conclusion. $[\alpha]_D$ had a significant increase with the improvement of the chiral component content. Furthermore, the Kuhn

dissymmetry factors $(g_{abs} = [CD/32\,980]/Abs)$ of P_X were calculated,[41,42] as listed in Table S5 (ESI†), to quantitatively evaluate the degree of preferential helicity. P_{55} showed a minimum g_{abs} value of -0.23×10^{-2}, and P_{91} had the highest g_{abs} value of -0.91×10^{-2}. The above results indicate that the copolymeric particles possess strong optical activity due to the one-handed helical conformation on the copolymer main chains.

Since the particles synthesized had the repeating unit structure of the fluorescent component, the resulting copolymeric particles P_X were expected to exhibit photoluminescence (PL) behavior (Fig. 2c). Thus, copolymeric particles were analyzed using fluorescence spectroscopy (Fig. 2b). We aimed to maintain the spherical shape of the particles during the process of characterizing the fluorescence emission, and so the particle/PVA composite films were directly tested using fluorescence spectroscopy. It should be noted that the optimal excitation wavelength is determined using the excitation spectra of the sample. As shown

176 | J. Mater. Chem. C, 2023, 11, 172–182

This journal is © The Royal Society of Chemistry 2023

in Fig. S9 (ESI†), taking P_{55}/PVA as a representative, the fluorescence excitation spectra were monitored at 430, 480, 500, 530, 550 and 600 nm. The optimal excitation wavelength was found to be constant at 365 nm at different emission wavelengths. The fluorescence spectra and CPL spectra were excited at 365 nm. The copolymeric particles with varying mass feed ratios all showed intense green emission (Fig. 2b) and had a maximum of 500 nm. Conversely, no fluorescence emission was found in the homopolymer P1. The fluorescent homopolymer P2 also showed a fluorescence emission peak at 500 nm. This result illustrates that the photoluminescence properties of the copolymeric particles are derived from the DA moieties (Fig. S10, ESI†). Moreover, the copolymeric particles showed an acceptable quantum yield of 7.3–39.8% (Table S5, ESI†). Among the particles, the fluorescence quantum yield of P_{55} was the highest, and its fluorescence intensity was the strongest. These results demonstrate that the fluorescence emission performance of copolymeric particles is stronger with an increase in the fluorescent components in a certain range.[43,44]

Based on the above data, we successfully prepared chiral fluorescent copolymeric particles. Similar to the CD and fluorescence tests, we aimed to maintain a satisfactory spherical shape of the particles while characterizing the CPL performance. Thus, the CPL properties of the resulting copolymeric particle P_X/PVA composite films were ultimately analyzed, as shown in Fig. 2d. Fortunately, relatively obvious CPL effects could be seen at 500 nm in P_X/PVA. Among them, the CPL effect of P_{91}/PVA was the most prominent, which was almost consistent with the regular pattern of the CD spectra. P_{55}/PVA exhibited the worst CPL signal of the tested particles. These data demonstrate that the intensity of the CPL signal is related to the CD effect. In order to further study the connection between the optically excited-state chirality and ground-state chirality, the relationship between the CPL property and CD effects was comprehensively investigated. We found that the line shape of the excitation fluorescence spectrum (Fig. S9, ESI†) was similar to that of the UV-vis absorption spectrum (Fig. 2a) of P_{55}/PVA. Meanwhile, obvious CD signals of P_{55}/PVA were observed at 340 nm. The results illustrate that the CPL signals may originate from the Cotton region at 340–400 nm. Specifically, P_{91}/PVA displayed a negative CD signal at 400 nm. P_{64}/PVA, P_{73}/PVA, and P_{82}/PVA exhibited negative CD signals at 340–400 nm. In addition, we quantitatively evaluated the CPL performance by calculating the luminescence asymmetry factor g_{lum} according to the equation $2 \times (I_L - I_R)/(I_L + I_R)$, where I_L and I_R represent the intensity of the left-handed and right-handed CPL, respectively.[45,46] Since the g_{lum} values rely on the intensity of PL and CPL, the maximum of g_{lum} uncertainty emerged at the corresponding position of CPL or PL extremum. The g_{lum} values of P_{55}/PVA, P_{64}/PVA, P_{73}/PVA, P_{82}/PVA, and P_{91}/PVA were -0.8×10^{-2}, -1.0×10^{-2}, -1.1×10^{-2}, -1.2×10^{-2} and -1.3×10^{-2}, respectively (Table S5, ESI†). Compared with the $|g_{lum}|$ value (1.4×10^{-3}) of the poly($1L_{0.9}$-co-$2_{0.1}$)-Boc copolymer solution in our previous work,[47] the P_{91} particle (1.3×10^{-2}) with a regular morphology ($\sim$610 nm in diameter) and narrow size distribution showed 9.3-fold amplification

through the self-assembly process. It is mainly due to the non-covalent bond synergy enhancing the CD effect at the same absorption region in solid aggregates. The above results illustrate that optically active helical copolymers may be used as a prominent candidate for constructing CPL solid materials.

Stimuli-responsive CPL behaviors of helical polymeric particles

The CPL helical polymeric particles P_X with a cis-transoidal main-chain structure are a type of typically dynamic helical substituted polyacetylene, and their conformations are sensitive to external stimuli owing to the low helix reversal barrier.[48,49] Thus, we investigated the influence of temperature and pH on the CD effect and CPL performance of the P_X/PVA composite films. The P_{55}/PVA composite film was used as a research representative. As shown in Fig. 3a and b, the CD and CPL intensities were reduced by 54.3% and 52.8%, respectively, as the temperature increased from 20 to 80 °C in the P_{55}/PVA composite film. The P_{55}/PVA composite film showed dynamic fluorescence behavior under different temperature conditions (Fig. 3d), which is consistent with the fluorescence emission in the CPL spectrum (Fig. 3b). This was because the helix-to-coil transition limited the chiral amplification of self-assembly and led to the emergence of the ACQ effect, as seen below in the section on mechanistic studies. Thus, the corresponding UV-vis absorption and fluorescence signals were significantly weakened with an increase in temperature. Remarkably, the CD and CPL signals both almost recovered to their original state (black line) on cooling the P_{55}/PVA composite film from 80 to 20 °C (cyan line). The g_{lum} values of the P_{55}/PVA composite film as a function of temperature are plotted in Fig. 3c. The g_{lum} value of the P_{55}/PVA composite film decreased by 53.4% as the temperature increased from 20 to 80 °C. These results indicate that the CD and CPL effects of the P_{55}/PVA composite film have sensitive and reversible temperature response capability.

Additionally, the effect of pH on the CD and CPL qualities of the P_{55}/PVA composite film was explored. P_{55}/PVA composite films were prepared with PVA aqueous solutions of varying pH values and analyzed using CD, UV-vis absorption, and CPL spectroscopy (Fig. 3e–g). The CD and CPL signals and g_{lum} value greatly decreased at 300–400 nm and 450–550 nm, under acidification (pH < 5) or alkalization (pH > 9). This showed that the helical structure of the SRCHPs was relatively stable when the pH value was close to neutral or weakly acidic. When the pH values were 1 and 3, the P_{55}/PVA composite film had null CD signals and the UV-vis absorption peak showed blue-shifts toward 310–320 nm. This suggested that the cis-transoidal helices became random coils after acidification. Thus, the P_{55}/PVA composite film also displayed no CPL signals and the fluorescence emission weakened with blue-shifts due to the influence of the random coil structure on the chiral amplification and AEE. By contrast, the CD and CPL signals at 300–400 nm decreased after alkalization but did not disappear when the pH was 9, 11, and 13. The UV-vis absorption and fluorescence emission peaks slightly red-shifted. This was because the cis-transoidal helices of P_{55} had an increase in helical pitch, which extended the backbone conjugation length.

This journal is © The Royal Society of Chemistry 2023

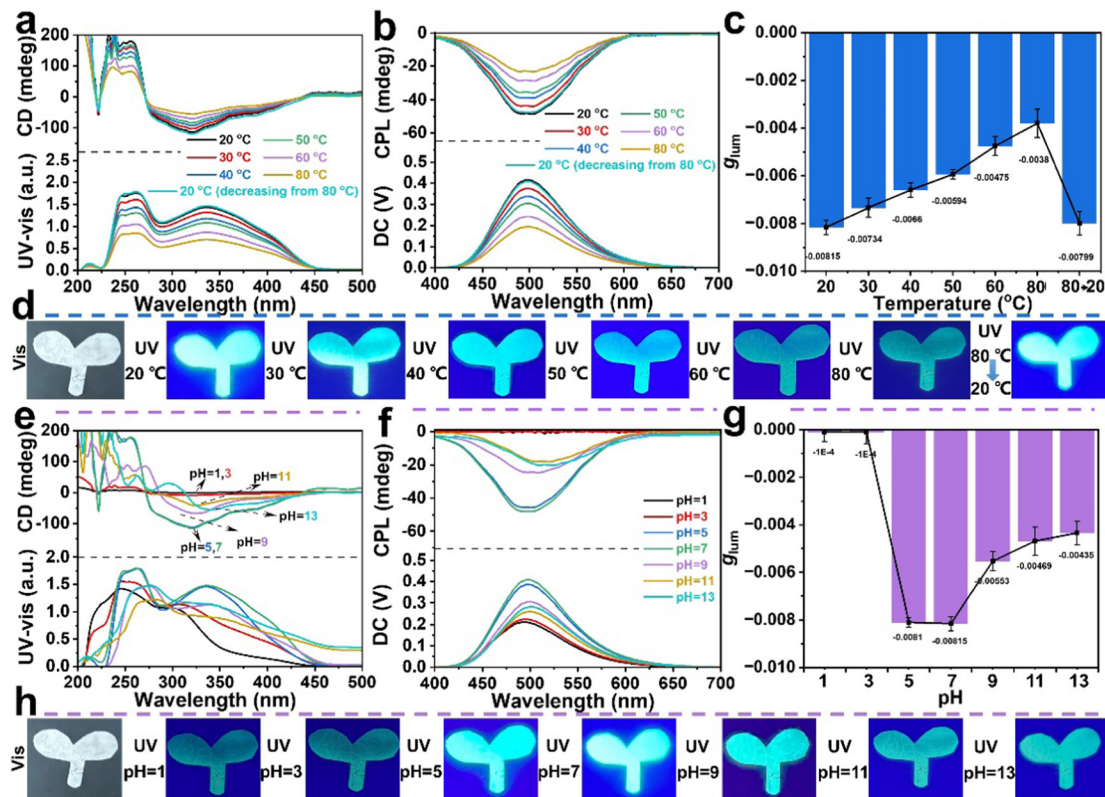*J. Mater. Chem. C*, 2023, **11**, 172–182 | **177**

Fig. 3 (a and e) CD and UV-vis absorption spectra, (b and f) CPL spectra excited at 365 nm, (c and g) CPL dissymmetry factor g_{lum}, and (d and h) dynamic fluorescent images of the P_{55}/PVA composite film with respect to varying temperature and pH values, respectively.

Meanwhile, the P_{55}/PVA composite film also exhibited dynamic fluorescence behavior under different pH conditions (Fig. 3h), which is consistent with the fluorescence emission in the CPL spectrum (Fig. 3f). Therefore, we can conclude that the P_{55}/PVA composite film is sensitive to pH. The typical dynamic cis-transoidal helical main chain of the polymer is the basic reason for the pH response.

The obvious CPL performance of chiral fluorescent copolymeric particles can be used as ultra-secure optical coding. Fig. 4 shows the anticounterfeiting phenomenon-based polarization of P_X/PVA composite films. A sapling-shaped pattern was composed of P_X/PVA composite films. Under natural light, the

sapling was visible on a black background (Fig. 4a). Under UV light of 365 nm wavelength, the sapling composed of P_X/PVA composite films presented fluorescence (Fig. 4b), which exhibited a first-line anti-counterfeiting feature. Fascinatingly, when observed under 365 nm UV light through a left-handed circular polarizer filter (LCPF) and a right-handed circular polarizer filter (RCPF), the obvious green fluorescence of the sapling was seen only with the LCPF but not with the RCPF (Fig. 4c and d), which showed a second-line anti-counterfeiting effect. LCPL emission enhanced the fluorescence emission of P_X, due to the LCPL activity of P_X, and RCPL emission weakened the fluorescence emission of P_X, owing to the RCPL activity of
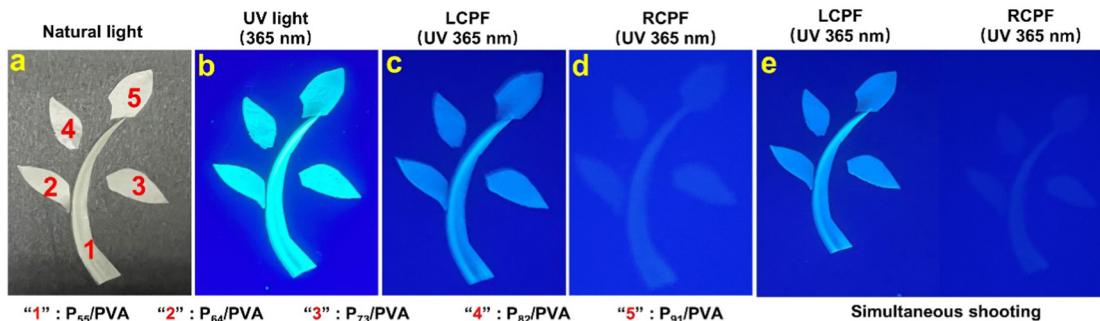

Fig. 4 Optical photos of latent patterns with different lighting conditions ((a) natural light; (b) UV light of 365 nm; (c) UV light of 365 nm under a left-handed circular polarizer filter; (d) UV light of 365 nm under a right-handed circular polarizer filter; (e) UV light of 365 nm under left and right-handed circular polarizer filters, simultaneously) of P_X/PVA composite films.

P$_X$. Fig. 4e displays the visible differences using one shot for left and right-handed circular polarizer filters, simultaneously, which further demonstrated the reliability of the second-line anti-counterfeiting effect. These findings demonstrate that P$_X$/PVA composite films can divide unpolarized fluorescence into two kinds of circularly polarized fluorescence. The P$_X$/PVA composite films are promising for application in super-secure communications and anticounterfeiting.

CPL stimuli-responsive and amplification mechanism

To explore the CPL stimuli-responsive mechanism of the copolymeric solid particles, the conformer structure of the copolymeric particles, owing to the close connection between the chiral photoelectric properties and conformers, was studied using resonance Raman and DSC characterization. Additionally, the CPL amplification mechanism was illustrated from the point of view of the conformer structure and the self-assembly driving force using FT-IR and fluorescence spectroscopy.

CPL stimuli-responsive mechanism. In the Raman spectra of the copolymeric particles (Fig. 5a), P$_X$ displayed two characterized vibration peaks of *cis* C=C bonds and naphthalene rings at 1618 and 1573 cm^{-1}, respectively.[50,52] However, P$_X$ did not exhibit the Raman peak belonging to *trans* C=C bonds. The characteristic vibration peaks of C–C and C–H bonds on the *cis* main chain at 1358, 1338 and 1000 cm^{-1} also appeared in the Raman spectrum of P$_X$.[51,52] Furthermore, the typical

characteristic vibration peak of *trans* C–C was observed at 1253 cm^{-1}. These results illustrate that P1 and P$_X$ take on typically dynamic cis-transoidal π-conjugated sequences.[53] P2 had an irregular geometric configuration. Meanwhile, as shown in Fig. 5b, the half-height width of P$_X$ was wider than that of P1, and the Raman peak of the *cis* C=C bonds in P$_X$ was red-shifted compared to that in P1. This result indicates that P$_X$ showed more morphological disorder and/or distorted structures than P1 due to the introduction of the dan sulfonamide group. Interestingly, P$_{55}$ had a smaller half-height width (64 cm^{-1}) than P$_{91}$ (81 cm^{-1}), P$_{82}$ (95 cm^{-1}), P$_{73}$ (96 cm^{-1}) and P$_{64}$ (99 cm^{-1}), due to an increase in the naphthalene content in dan sulfonamide (M2). This suggests that P$_{55}$ can adopt the most ordered dynamic cis-transoidal helix, resulting in stimuli-responsive CD and CPL effects.

The cis-transoidal helix of the SRCHPs was further confirmed using DSC traces (Fig. 5c). Pure P1 and P$_X$ both presented an exothermic peak at 240 °C, attributed to the thermal isomerization from cis-transoid to trans-transoid, according to the work by Percec and co-workers.[54–56] This phenomenon demonstrated that P1 and P$_X$ underwent the geometric conformation of a cis-transoid. The isomerization temperatures from cis-transoid to trans-transoid of P$_X$ and P2 were lower than those of P1, which is attributed to the lack of persistent conjugate length on the one-handed helical main chain.[57,58] However, P$_{55}$ (238 °C) had a higher transition temperature from
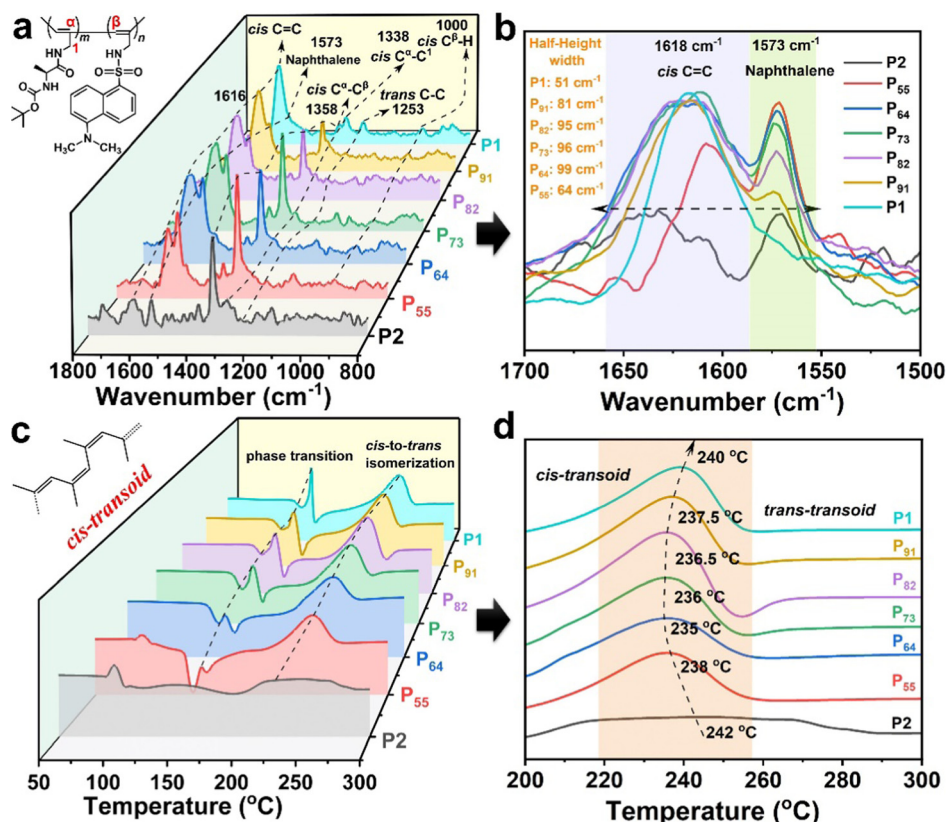

Fig. 5 (a) Resonance Raman spectra and (b) partial resonance Raman spectra (C=C stretching region) using a 325 nm excitation laser pulse; (c and d) DSC traces (N$_2$, 10 °C min^{-1}) of P1, P2 and P$_X$.

cis-transoid to trans-transoid than P_{64} (235 °C), P_{73} (236 °C), P_{82} (236.5 °C), and P_{91} (237.5 °C). This indicates that P_{55} take on a dynamic cis-transoidal helical structure with a more regular geometric configuration and higher thermal stability. Therefore, the CPL stimuli-responsive mechanism of the SRCHPs can be attributed to the fact that the external stimuli of temperature or pH may be affected by the dynamic cis-transoidal helix of the substituted polyacetylene backbone.

CPL amplification mechanism. The geometric configuration of the copolymeric particles and the driving force of self-assembly were also studied by FT-IR spectroscopy. As presented in Fig. 6a, there emerged noticeable vibration characteristic vibration peaks of *trans* C–H (1457 and 1316 cm^{-1}), *trans* C–C (787 cm^{-1}), *cis* C–H (1392 and 1123 cm^{-1}), *cis* polymer (875 cm^{-1}), and C–H bonds of naphthalene rings (628 cm^{-1})[59–63] in the FT-IR spectra of P_X and P1. The characteristic peaks of *cis* C–H and the *cis* polymer in the backbone of P2 were hardly observed. These facts clearly demonstrate that P1 and P_X form the geometric configuration of a dynamic cis-transoidal helix. Furthermore, the vibration intensities of *cis* C–H and the *cis* polymer in P_X became weaker with the increase in the dan sulfonamide content, whereas the vibration intensities of *trans* C–H and *trans* C–C in P_X turned stronger. This means that the helical configuration of the copolymeric particles had increasing *trans* fragments with an increase in dan sulfonamide and a decrease in amino acid amide contents. Fig. 6b also presents the same phenomenon, where P_{55} has the most *trans* C–C bonds at 1635 cm^{-1}. Excitingly, P1 showed an intense vibration characteristic peak at 1672 cm^{-1} and a low shoulder peak at 1682 cm^{-1}

originating from the C=O vibration, whereas P_{91}, P_{82}, P_{73}, P_{64} and P_{55} presented almost the same vibration for these peaks. Compared with P1, a significant decrease of the second C=O vibration peak and the slight blue-shift of the N–H vibration peak from 1537 to 1541 cm^{-1} in P_X implies that the intramolecular hydrogen bond became weakened between the C=O and N–H bonds due to the existence of dan sulfonamide, wherein the large steric group increased the distance between the side groups.[61,63] However, P_{55} had a closer location with P1 at 1538 cm^{-1} compared to P_{91}, P_{82}, P_{73}, and P_{64}, which explains why P_{55} incurred new hydrogen bonding, as shown in Fig. 6c. The hydrogen bond played a vital role in stabilizing the cis-transoidal helical conformation.

Interestingly, P_X with cis-transoidal helical conformation did not have an ACQ effect. P_X still exhibited intense fluorescence emission on excitation at 260 nm (Fig. S11, ESI†), which was tied to the absorption of side groups. This illustrates that the amide groups and naphthalene rings were conjugated with the copolymer main chain. The energy was absorbed and transferred from the dan sulfonamide side group to the main chain through this conjugate structure bridge, further resulting in the AEE effect and fixing the cis-transoid helix. Therefore, the CPL amplification of the SRCHPs originates from the driving force of hydrogen bonding and the conjugated interaction.

Overall, these characterization studies prove that at a large scale, the coordination of the intramolecular hydrogen bonding and conjugated π–π stacking interactions based on the cis-transoidal helical conformation results in a stimuli-responsive
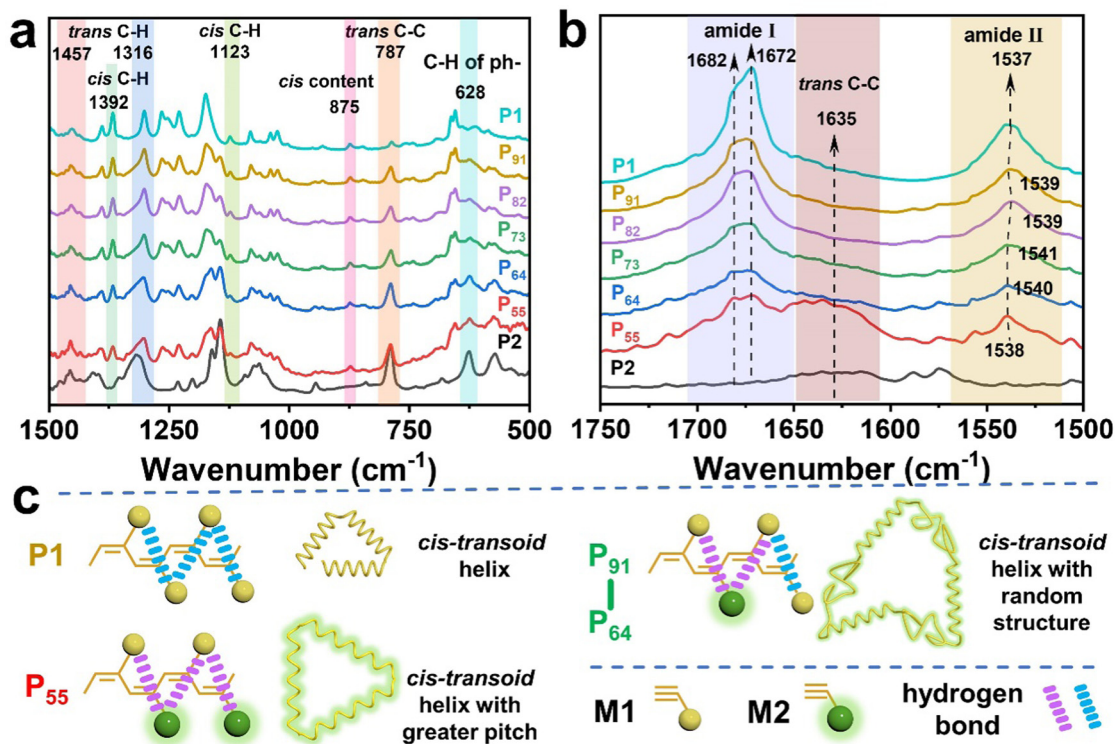

Fig. 6 (a and b) Partial FT-IR spectra (1500–500 and 1750–1500 cm^{-1} regions, KBr pallet), and (c) proposed structure of P_X.

and remarkably amplified CPL signal of copolymeric particles. Furthermore, the amide substituents and naphthalene rings in our design provide strong intramolecular hydrogen bonds and conjugated π–π stacking interactions. The cis-transoidal helical structures endow the main chain with the AEE effect and dynamic helicity.

Conclusions

Stimuli-responsive helical polymeric particles (SRHPs) that have a spherical morphology with high yields and CPL performance were successfully synthesized *via* precipitation copolymerization of chiral and fluorescent acetylenic monomers. The SRHPs perfectly combined the special helical conjugated structure, fluorescent component, and polymeric macroparticles in one entity. Furthermore, the formation mechanism and main influencing factors of the SRHPs were summarized. The $|g_{lum}|$ value (1.3×10^{-2}) of the P_{91} SRHPs exhibited 9.3-fold amplification compared to that of a copolymer solution of poly($1L_{0.9}$-co-$2_{0.1}$)-Boc (1.4×10^{-3}). More importantly, the SRHPs not only exhibited temperature-responsive and pH-responsive CPL properties but also presented potential applications in information encryption and anticounterfeiting. The CPL stimuli-responsive and amplification mechanism followed the coordination of the intramolecular hydrogen bonding and conjugated π–π stacking interactions at a large scale based on the dynamic cis-transoidal helix. This investigation provides new insights into the future development of stimuli-responsive CPL solid materials with amplified CPL properties.

Author contributions

J. W. Li and D. M. Qi constructed the project. H. M. Duan and H. K. Pan designed and prepared the materials. D. M. Qi and H. M. Duan carried out the characterization studies and proposed suggestions for the work. J. W. Li and H. M. Duan co-wrote the manuscript with the contribution and approval of all of the authors. All authors discussed and commented on the manuscript.

Conflicts of interest

There are no conflicts to declare.

Acknowledgements

References

1 Y. D. Chen, P. Lu, Z. Y. Yuan, Q. Ye and H. L. Zhang, *ACS Appl. Mater. Interfaces*, 2020, **12**, 56604–56614.

2 M. Seitz, E. G. Moore, A. J. Ingram, G. Muller and K. N. Raymond, *J. Am. Chem. Soc.*, 2007, **129**, 15468–15470.

3 H. Maeda, Y. Bando, K. Shimomura, I. Yamada, M. Naito, K. Nobusawa, H. Tsumatori and T. Kawai, *J. Am. Chem. Soc.*, 2011, **133**, 9266–9269.

4 Z. Cui, J. Ding, Y. Gao and F. Li, *CCS Chem.*, 2022, **4**, 2953–2958.

5 Q. Xia, W. W. Xie, T. C. He, H. Y. Zhang, Z. J. Zhao, G. X. Huang, B. S. Li and B. Z. Tang, *CCS Chem.*, 2022, DOI: **10.31635/ccschem.022.202202173**.

6 A. Ikenaga, Y. Akiyama, T. Ishiyama, M. Gon, K. Tanaka, Y. Chujo and K. Isoda, *ACS Appl. Mater. Interfaces*, 2021, **13**, 47127–47133.

7 H. Li, H. H. Li, W. Wang, Y. Tao, S. Wang, Q. Q. Yang, Y. B. Jiang, C. Zheng, W. Huang and R. F. Chen, *Angew. Chem.*, 2020, **59**(12), 4756–4762.

8 P. Kanoo, R. Haldar, S. K. Reddy, A. Hazra, S. Bonakala, R. Matsuda, S. Kitagawa, S. Balasubramanian and T. K. Maji, *Chem. – Eur. J.*, 2016, **22**, 15864–15873.

9 H. L. Yu, B. Zhao, J. B. Guo, K. Pan and J. P. Deng, *J. Mater. Chem. C*, 2020, **8**, 1459–1465.

10 H. Maeda, Y. Y. Bando, K. Shimomura, I. Yamada, M. Naito, K. Nobusawa, H. Tsumatori and T. Kawai, *J. Am. Chem. Soc.*, 2011, **133**, 9266–9269.

11 L. K. Ji, Y. Zhao, M. Tao, H. X. Wang, D. Niu, G. H. Ouyang, A. D. Xia and M. H. Liu, *ACS Nano*, 2020, **14**, 2373–2384.

12 F. Wang, F. W. Gan, C. S. Shen and H. B. Qiu, *J. Am. Chem. Soc.*, 2020, **142**, 16167–16172.

13 Q. Li and Z. Li, *Acc. Chem. Res.*, 2020, **53**, 962–973.

14 C. H. Zhang, H. Y. Dong and Y. S. Zhao, *Adv. Opt. Mater.*, 2018, **6**, 1701193.

15 P. P. Li, H. Z. Gao, B. Zhao and J. P. Deng, *Adv. Mater.*, 2022, **34**, 7503–7515.

16 K. Velmurugan, A. Murtaza, A. Saeed, J. Li, K. Wang, M. Zuo, Q. Liu and X. Y. Hu, *CCS Chem.*, 2022, **4**, 3426–3439.

17 H. Zhong and J. P. Deng, *Polym. Rev.*, 2022, 1–34.

18 J. Kumar, T. Nakashima and T. Kawai, *J. Phys. Chem. Lett.*, 2015, **6**, 3445–3452.

19 F. Li, Y. X. Wang, Z. Y. Wang, Y. X. Cheng and C. J. Zhu, *Polym. Chem.*, 2015, **6**, 6802–6805.

20 S. W. Zhang, Y. Sheng, W. Guo, Y. W. Quan, Y. X. Cheng and C. J. Zhu, *Polym. Chem.*, 2015, **6**, 2416–2422.

21 G. A. Hembury, V. V. Borovkov and Y. Inoue, *Chem. Rev.*, 2008, **108**, 1–73.

22 Y. J. Zhang and J. P. Deng, *Polym. Chem.*, 2020, **11**, 5407–5423.

This journal is © The Royal Society of Chemistry 2023

J. Mater. Chem. C, 2023, **11**, 172–182 | **181**

23 Z. W. Luo, L. Tao, C. L. Zhong, Z. X. Li, K. Lan, Y. Feng, P. Wang and H. L. Xie, *Macromolecules*, 2020, **53**, 9758–9768.

24 Y. Liu, A. J. Qin and B. Z. Tang, *Prog. Polym. Sci.*, 2018, **78**, 92–138.

25 B. Zhao, K. Pan and J. P. Deng, *Macromolecules*, 2018, **51**, 7104–7111.

26 L. J. Yin, H. M. Duan, T. Chen, D. M. Qi and J. P. Deng, *Polym. Chem.*, 2021, **12**, 6404–6416.

27 B. Zhao, X. B. Gao, N. Lu and J. P. Deng, *Adv. Opt. Mater.*, 2020, **8**, 2000858.

28 D. Lee, Y.-J. Jin, H. Kim, N. Suzuki, M. Fujiki, T. Sakaguchi, S. K. Kim, W.-E. Lee and G. Kwak, *Macromolecules*, 2012, **45**, 5379–5386.

29 B. A. San Jose, J. Yan and K. Akagi, *Angew. Chem., Int. Ed.*, 2014, **126**, 10817–10820.

30 S. Wang, D. P. Hu, X. Y. Guan, S. L. Cai, G. Shi, Z. G. Shuai, J. Zhang, Q. Peng and X. H. Wan, *Angew. Chem., Int. Ed.*, 2021, **60**, 21918–21926.

31 H. J. Huang, C. N. Chen, D. Y. Zhang, J. P. Deng and Y. P. Wu, *Macromol. Rapid Commun.*, 2014, **35**, 908–915.

32 Y. J. Zhang, J. P. Deng and K. Pan, *Macromolecules*, 2018, **51**, 8878–8886.

33 G. Z. Gao, F. Sanda and T. Masuda, *Macromolecules*, 2003, **36**, 3938–3943.

34 R. R. Schrock and J. A. Osborn, *Inorg. Chem.*, 1970, **9**, 2339–2343.

35 H. J. Huang, W. T. Yang and J. P. Deng, *RSC Adv.*, 2015, **5**, 26236–26245.

36 J. Tabei, R. Nomura and T. Masuda, *Macromolecules*, 2003, **36**, 573–577.

37 J. P. Deng, J. Tabei, M. Shiotsuki, F. Sanda and T. Masuda, *Macromolecules*, 2004, **37**, 1891–1896.

38 F. Freire, J. M. Seco, E. Quiñoá and R. Riguera, *Angew. Chem., Int. Ed.*, 2011, **50**, 11692–11696.

39 J. P. Deng, J. Tabei, M. Shiotsuki, F. Sanda and T. Masuda, *Macromolecules*, 2004, **37**, 5149–5154.

40 D. Hirose, A. Isobe, E. Quiñoá, F. Freire and K. Maeda, *J. Am. Chem. Soc.*, 2019, **141**, 8592–8598.

41 J. van Gestel, A. R. A. Palmans, B. Titulaer, J. A. J. M. Vekemans and E. W. Meijer, *J. Am. Chem. Soc.*, 2005, **127**, 5490–5494.

42 S.-Y. Kim, M. Fujiki, A. Ohira, G. Kwak and Y. Kawakami, *Macromolecules*, 2004, **37**, 4321–4324.

43 S. S. Chen, T. Han, J. K. Liu, X. T. Liang, J. L. Yang and B. Z. Tang, *J. Mater. Chem. A*, 2022, **10**, 15438–15448.

44 X. J. Wan, S. Yao, H. Y. Liu and Y. W. Yao, *J. Mater. Chem. A*, 2013, **1**, 10505–10512.

45 J. P. Riehl and F. S. Richardson, *Chem. Rev.*, 1986, **86**, 1–16.

46 Y. J. Deng, M. Z. Wang, Y. L. Zhuang, S. J. Liu and Q. Zhao, *Light: Sci. Appl.*, 2021, **10**, 1–18.

47 H. M. Duan, C. J. Zhu, D. M. Qi and J. W. Li, *Polymer*, 2022, **255**, 125123.

48 K. Maeda, H. Mochizuki, M. Watanabe and E. Yashima, *J. Am. Chem. Soc.*, 2006, **128**, 7639–7650.

49 Z. W. Ma, B. Zhao, Y. S. Gong, J. P. Deng and Z. A. Tan, *J. Mater. Chem. A*, 2019, **7**, 22826–22847.

50 S. Wang, X. Y. Feng, Z. Y. Zhao, J. Zhang and X. H. Wan, *Macromolecules*, 2016, **49**, 8407–8417.

51 A. Motoshige, Y. Mawatari, Y. Yoshida, R. Motoshigea and M. Tabata, *Polym. Chem.*, 2014, **5**, 971–978.

52 S. Leiras, F. Freire, J. M. Seco, E. Quiñoá and R. Riguera, *Chem. Sci.*, 2013, **4**, 2735–2743.

53 G. Z. Gao, F. Sanda and T. Masuda, *Macromolecules*, 2003, **36**, 3932–3937.

54 V. Percec, J. G. Rudick, M. Peterca and P. A. Heiney, *J. Am. Chem. Soc.*, 2008, **130**, 7503–7508.

55 V. Percec, J. G. Rudick, M. Peterca, M. Wagner, M. Obata, C. M. Mitchell, W.-D. Cho, V. S. K. Balagurusamy and P. A. Heiney, *J. Am. Chem. Soc.*, 2005, **127**, 15257–15264.

56 C. I. Simionescu and V. Percec, *Prog. Polym. Sci.*, 1982, **8**, 133–214.

57 L. J. Liu, T. Namikoshi, Y. Zang, T. Aoki, S. Hadano, Y. Abe, I. Wasuzu, T. Tsutsuba, M. Teraguchi and T. Kaneko, *J. Am. Chem. Soc.*, 2013, **135**, 602–605.

58 A. Motoshige, Y. Mawatari, Y. Yoshida, C. Seki, H. Matsuyama and M. Tabata, *J. Polym. Sci., Part A: Polym. Chem.*, 2012, **50**, 3008–3015.

59 S. L. Hsu, A. J. Signorelli, G. P. Pez and R. H. Baughman, *J. Chem. Phys.*, 1978, **69**, 106–111.

60 Y. Mawatari, A. Motoshige, Y. Yoshida, R. Motoshige, T. Sasaki and M. Tabata, *Polymer*, 2014, **55**, 2356–2361.

61 D. Liu, H. Y. Chen, J. P. Deng and W. T. Yang, *J. Mater. Chem. C*, 2013, **1**, 8066–8074.

62 S. Liu, B. Yu and T. Zhong, *J. Mater. Chem. A*, 2013, **1**, 13314–13320.

63 Z. X. Xu, K. Liu, H. Huang, Y. D. Zhang, Z. Y. Long, M. M. Tong and G. J. Chen, *J. Mater. Chem. A*, 2022, **10**, 5540–5549.

182 | *J. Mater. Chem. C*, 2023, **11**, 172–182

This journal is © The Royal Society of Chemistry 2023